nature physics

Review article

https://doi.org/10.1038/s41567-024-02679-7

Quantum critical metals and loss of quasiparticles

Received: 10 December 2023

Accepted: 24 September 2024

Haoyu Hu[1,2], **Lei Chen**[1] & **Qimiao Si**[1]

Strange metals develop near quantum critical points in a variety of strongly correlated systems. Some of the issues that are central to the field include how the quantum critical state loses quasiparticles, how it drives superconductivity and to what extent the strange-metal physics in different classes of correlated systems are interconnected. In this Review, we survey some of these issues from the vantage point of heavy-fermion metals. We describe the notion of Kondo destruction and how it leads to several crucial effects. These include a transformation of the Fermi surface from large to small when the system is tuned across the quantum critical point, a loss of quasiparticles everywhere on the Fermi surface when it is perched at the quantum critical point and a dynamical Planckian scaling in various physical properties including charge responses. We close with a discussion about the connections between the strange-metal physics in heavy-fermion metals and its counterparts in the cuprates and other correlated materials.

Large classes of quantum materials host strongly correlated electrons[1,2] and many of them feature unconventional superconductivity. One connection among the strongly correlated systems is illustrated in Fig. 1a, which shows the superconducting transition temperature T_c and the effective Fermi temperature T_0, the temperature for Fermi degeneracy, for various strongly correlated superconductors. The ratio of T_c/T_0 is several per cent, with each temperature scale spanning about three decades. This qualifies these systems as high-T_c superconductors, given that this ratio is about two orders of magnitude smaller in conventional superconductors. Another connection lies in their normal states at temperatures above the superconducting transition temperature (so, when $T > T_c$), which are often strange metals that have an electrical resistivity that is linear in temperature and a slew of other exotic properties.

The link between the strange-metal normal state and unconventional superconductivity in heavy-fermion systems, which are characterized by electronic excitations whose effective masses are orders of magnitude larger than the free electron mass, is particularly striking. Indeed, heavy-fermion metals represent a prototypical setting in which quantum critical metallicity has been elucidated[3], in part because T_c is relatively small in absolute magnitude in these materials, so it opens up a large window of temperature over which the strange-metal properties can be explored. These systems often have antiferromagnetic (AF) correlations. The existence of heavy-fermion superconductors is a venerable topic, and this material family has now grown to about 50 members. In contrast, the strange-metal behaviour and its association with quantum criticality have been the focus only relatively recently.

It is natural for quantum criticality to drive unusual properties[4]. Indeed, as a system is tuned towards its quantum critical regime at a given low (but non-zero) temperature, the entropy is expected to be maximized[5,6]. This behaviour was demonstrated in ref. 7 and is illustrated in Fig. 1b, which presents the experimental observations in $CeCu_{6-x}Au_x$ as a function of multiple tuning parameters. Tuning the system in the directions that are orthogonal to the gradient of entropy, the distance to the quantum critical point (QCP) remains unchanged. The gradient of the entropy vanishes precisely at the QCP, which indicates the accumulation of entropy in the quantum critical regime. In this sense, quantum critical systems are particularly soft and are prone to the formation of unusual excitations and exotic phases.

That strange metals develop via quantum criticality is clearly demonstrated in heavy-fermion metals. We illustrate the point in $YbRh_2Si_2$ and $CeRhIn_5$, via their respective phase diagrams shown in Fig. 1c,d. The quantity γ—which is plotted as the colour scale—represents the exponent of the resistivity's dependence on temperature, so regions where $\gamma \approx 1$ represent the strange-metal regime. Both materials show an AF order at ambient conditions. In $YbRh_2Si_2$, a magnetic field applied

---

[1] Department of Physics and Astronomy, Extreme Quantum Materials Alliance, Rice University, Houston, TX, USA. [2] Donostia International Physics Center, Donostia-San Sebastian, Spain. e-mail: huhaoyu314@gmail.com; lc73@rice.edu; qmsi@rice.edu

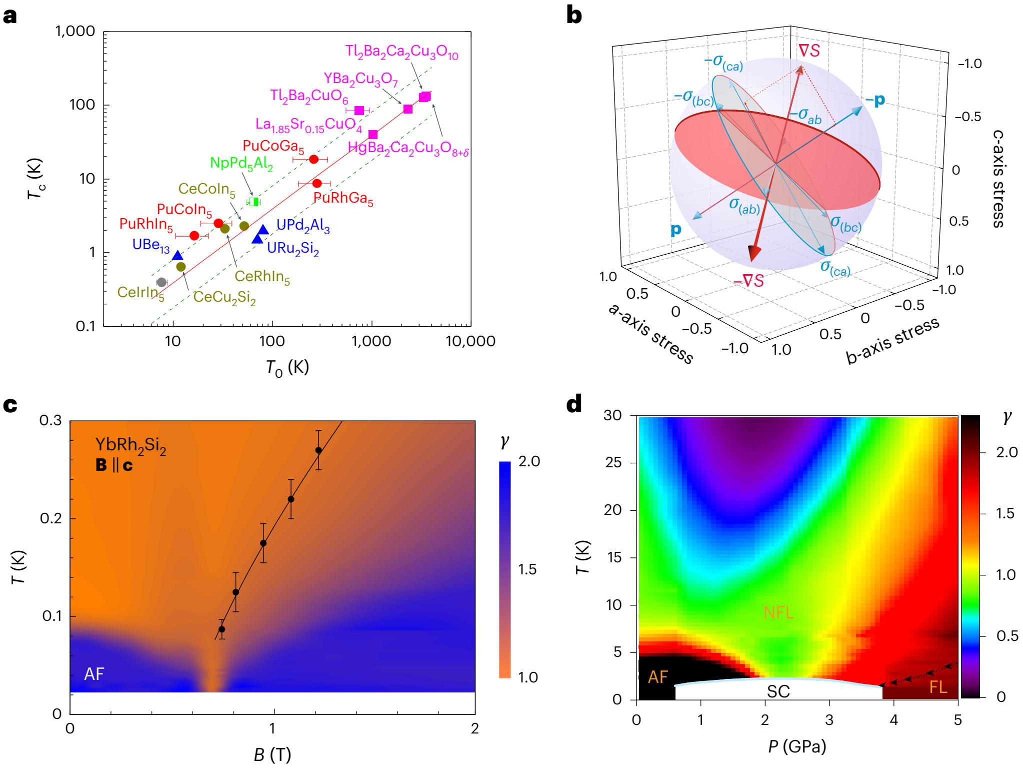

Fig. 1 | Strange metallicity and superconductivity. a, Superconducting transition temperature (T_c) versus the effective Fermi temperature (T_0, extracted from entropy and other means) for various superconductors from different material families. The red solid line indicates the linear proportionality between the two temperature scales. All materials, marked by the different colours and symbols, approximately follow this behaviour and are located within the region bounded by the two green dashed lines. The error bars reflect the uncertainties in the measurements and analyses. **b**, Illustration of the evolution in the entropy near a QCP, based on measurements of the uniaxial Grüneisen ratios in $CeCu_{6-x}Au_x$ at its critical concentration $x_c = 0.1$. Shown here is the parameter space of the uniaxial stress (p) along the crystalline $ab\,c$ axis. $\sigma_{(ab)}$ represents the shear pressure. The red arrow marks the direction with the steepest slope of entropy ∇S, with the directions perpendicular to it marked by the red plane. **c**,**d**, Temperature-control parameter phase diagrams of $YbRh_2Si_2$ under a magnetic field (B) applied along the crystalline c direction of the system[8,112] (**c**) and $CeRhIn_5$ under pressure (P)[13] (**d**). The colours represent the temperature exponent γ of the resistivity (ρ), determined by a logarithmic derivative of $\Delta\rho(T) \equiv \rho(T) - \rho(T = 0)$ with respect to log$T$, signifying a T^γ dependence. In panel **c**, the black solid line tracks the evolution in the Hall coefficient and thermodynamic quantities that indicate a crossover between large and small Fermi surfaces. The error bars reflect the uncertainty of the extracted crossover location. In panel **d**, the phase boundaries are displayed for the local-moment antiferromagnetic (AF) order, the superconducting (SC) phase, and the regions (below the black dotted line) where the resistivity follows a T^2 temperature dependence, characteristic of a Landau Fermi liquid (FL). The cone-shaped green region denotes the non-Fermi liquid (NFL) regime with a sub-linear T-dependence in the resistivity. Panels adapted with permission from: **a**, ref. 111, Springer Nature Ltd; **b**, ref. 7, Springer Nature Ltd; **c**, 112, Springer Nature Ltd; **d**, ref. 13, Springer Nature Ltd.

perpendicular to its tetragonal plane of about 0.7 T (or one applied within the plane of about 66 mT) tunes the system to its QCP[8], where a T-linear resistivity[9] occurs over more than three decades in temperature[10]. In $CeRhIn_5$, a quantum critical fan develops near a pressure of 2.3 GPa (refs. 11,12) with a nearly T-linear resistivity[13].

Theories of metallic QCPs have two general types. One class of theory is based on the fluctuations of Landau's order parameter, as described by the Hertz–Millis–Moriya approach[14,15]. Typically, this order parameter corresponds to a spin-density-wave (SDW) order at an AF wavevector **Q**. In this case, the non-zero ordering wavevector **Q** links narrow hot regions of the Fermi surface to each other. The order-parameter fluctuations couple to electrons from a small portion (hot region) of the Fermi surface, as shown in Fig. 2. Meanwhile, the majority of the Fermi surface remains cold in the sense that the order-parameter fluctuation connects one point on the cold region of the Fermi surface to another point in the Brillouin zone where the energy level lies substantially away from the Fermi energy. Correspondingly, for the electronic states in the cold region of the Fermi surface, the quantum critical fluctuations have a minimal effect and the quasiparticles retain their integrity[16–18]. The electrical transport will not show the strange-metal behaviour given that the quasiparticles, being long-lived, will short-circuit the electrical transport.

To realize the strange-metal behaviour, it is necessary to destroy the quasiparticles on the entire Fermi surface. This takes place in the second type of theory for metallic quantum criticality, which goes beyond the Landau framework[19–21].

Here we survey the beyond-Landau quantum criticality. We start by considering how quasiparticles can be critically destroyed. The central theme here is that, for bad metals such as heavy-fermion systems, the quasiparticles are fragile to begin with and their formation takes place through a process that is non-perturbative in electron correlations, and yet well understood. This understanding sets the stage for confronting the central challenge, which is how the quasiparticles are lost. For heavy-fermion metals, the Kondo effect underlies the formation of heavy quasiparticles, whereas the Kondo destruction leads to their suppression. We suggest that these understandings are relevant to the loss of quasiparticles in a variety of strongly correlated systems, including the doped cuprates, the iron chalcogenides and certain organic superconductors. In addition to surveying the theoretical issues, we describe some of the salient experimental developments[22–28].

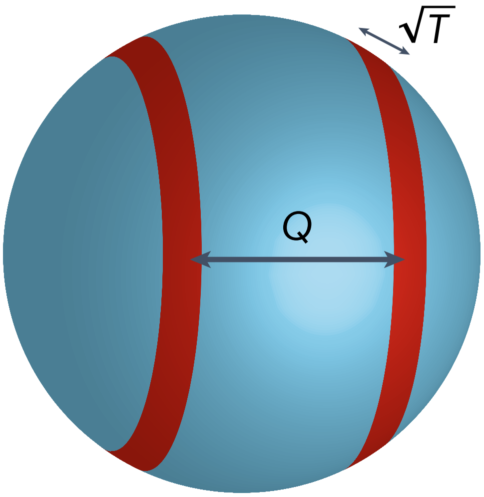

Fig. 2 | Schematic illustration of the Fermi surface for an SDW QCP. States in a small portion of the Fermi surface (red stripes with a width of the order of $\sqrt{T}$ for three dimensions) can be scattered by the low-energy critical bosons of wavevector **Q**. These states are hot in that they experience strong scattering by the order-parameter fluctuations. Meanwhile, the majority of the Fermi surface remains cold (blue region), where Landau quasiparticles are left intact. The electrical transport is dominated by the contributions from the cold region of the Fermi surface and therefore will not show strange-metal behaviour.

Quantum critical metals: how to destroy quasiparticles

Robust and fragile quasiparticles

For quantum many-body systems, the physics at low energies is analysed in terms of building blocks and their symmetry-allowed interactions[2]. Traditionally, one takes bare electrons as the building blocks and treats the electron–electron interactions order by order in perturbation theory[29]. The notion of quasiparticles survives up to infinite order of the perturbation series. In that sense, quasiparticles are rather robust. For a long time, the validity of Fermi liquid theory was largely unquestioned for systems in dimensions higher than one; indeed, a Fermi liquid was considered to be the only fixed point of the renormalization-group (RG) flow in such dimensions[30,31]. A quasiparticle corresponds to a sharp peak in the electron spectral function as a function of energy for a fixed wavevector. The wavevectors of zero-energy excitations form a Fermi surface; the volume enclosed by the Fermi surface, according to Luttinger's theorem, is proportional to the number of the underlying electrons even in the presence of interactions[32]. The quasiparticle has the physical meaning of a dressed electron; its quantum numbers are exactly those of a bare electron or hole, namely, charge $\pm e$ and spin-$\hbar/2$, where $\hbar$ is the reduced Planck constant. Their Fermi statistics dictates a decay rate that goes as $(k_\mathrm{B}T)^2$, where k_B is the Boltzmann constant, or as E^2 as the energy measured from the Fermi energy, E, goes to zero. In the language of Green's functions, the momentum $\mathbf{k}$ and frequency ω-dependent self-energy $\Sigma(\mathbf{k}, \omega)$ retains the Fermi liquid form up to infinite orders of the perturbative expansion[29]. This turns out to ensure a non-zero value for the quasiparticle weight, $Z_\mathbf{k}$.

Sufficiently strong electron correlations can lead to more suitable choices for the building blocks of the low-energy physics. For example, heavy-fermion systems involve local *f*-electron-derived moments and itinerant *spd*-electron bands as the starting point for the description of their low-energy properties[2,3,33–35]. In that case, quasiparticles are fragile, with a weight that is exponentially small.

An example is given by the Kondo-lattice Hamiltonian, which is described in Box 1. We start from the parameter regime when the Kondo interaction between the local moments and the itinerant electrons succeeds in driving the formation of a Kondo singlet, which can be pictured as a bound state between a local moment and a triplet particle–hole combination of the conduction electrons. Breaking the bound state leads to not only bare conduction electrons but also a composite heavy fermion formed between the local moment and a conduction electron. The composite fermions have the same quantum numbers as bare electrons, and they hybridize with the conduction electrons to form heavy quasiparticles. These quasiparticles have a large effective mass and a small quasiparticle weight Z that is exponentially small and, in practice, is of the order 10^{-3}.

When the quasiparticles are this fragile, competing interactions can readily destroy them.

Quantum criticality from Kondo destruction

The notion of Kondo-destruction quantum criticality invokes fluctuations that go beyond a Landau order parameter. For Kondo-lattice systems, it captures the dynamical competition between the Kondo interaction described above and RKKY interactions, which are interactions between the local moments mediated by the spins of the itinerant electrons, as described in Box 1. The corresponding QCP[3,19] is illustrated in Fig. 3a, in the space of temperature and the non-thermal control parameter, $\delta = T_\mathrm{K}^0/I$, which is the ratio of the bare Kondo temperature to the RKKY interaction I.

When δ is sufficiently large, the Kondo interaction dominates and a Kondo singlet is formed in the ground state, as illustrated in Fig. 3c. As the RKKY interaction is increased, meaning when the parameter δ is tuned downwards, the RKKY interaction becomes important and promotes correlations of a spin singlet between the local moments. This process is detrimental to the formation of the Kondo singlet. When it suppresses the Kondo singlet in the ground state, the composite heavy quasiparticles are lost.

Thus, both the formation and loss of quasiparticles can be considered by analysing the fate of the Kondo singlet or, more specifically, the amplitude of the Kondo singlet in the ground state. Our strategy is to start from the Kondo side, and see whether and how the dynamical competition of the RKKY interaction brings about the suppression of this Kondo-singlet amplitude. One can, in principle, also work from the opposite end, by analysing the Kondo lattice in terms of a quantum nonlinear sigma model representation; the results of such analyses[36–43] are consistent with the conclusions we present here.

Box 1 provides further details on how the dynamical competition from the RKKY interactions suppresses the Kondo singlet and, by extension, quasiparticles. The key is a new fixed point, marked red in panel b of Box 1 figure. Here, the Kondo-singlet amplitude vanishes in the ground state, and the weight of the Landau quasiparticle goes to zero. This fixed point is interacting (as opposed to Gaussian), where $k_\mathrm{B}T$ is the only energy scale.

Global phase diagram

The introduction of Kondo destruction has inspired considerations of new quantum phases in the AF Kondo-lattice systems. These phases are distinguished not only by the Landau order parameters but also by the existence or absence of the Kondo singlet in the ground state. This has led to a global phase diagram[36,44,45], as shown in Fig. 4, in the two-parameter space of J_K, the Kondo coupling, and G, which specifies the extent of the quantum fluctuations in the local-moment magnetism. The G axis captures the tuning of dimensionality[46] or geometrical frustration[47–50]. The quantum phases are distinguished by their magnetic behaviour and the size of their Fermi surfaces. Here, P and AF represent the paramagnetic and AF phases, respectively, and the subscripts S and L denote small and large Fermi surface, respectively. As we explain in Box 1, a large Fermi surface denotes that both the local moments and conduction electrons contribute to the Fermi volume through the Kondo effect, whereas a small Fermi surface signifies the absence of the Kondo effect, with only the conduction electrons contributing to the Fermi volume.

BOX 1

Kondo-lattice system

Consider the Kondo-lattice Hamiltonian:

$$H_{\mathrm{KL}}=\sum_{\mathbf{k},\sigma}\varepsilon_{\mathbf{k}}c^{\dagger}_{\mathbf{k}\sigma}c_{\mathbf{k}\sigma}+\sum_{ij}I_{ij}\mathbf{S}_i\cdot\mathbf{S}_j+\sum_i J_{\mathrm{K}}\mathbf{S}_i\cdot c_i^{\dagger}\frac{\boldsymbol{\sigma}}{2}c_i. \qquad (6)$$

The involved building blocks are the *f* electrons in the form of local moments, $\mathbf{S}_i$, and a band of *spd* conduction electrons, $c_{\mathbf{k}\sigma}$ with an energy dispersion $\varepsilon_{\mathbf{k}}$. At each site *i*, an AF Kondo interaction J_{K} couples the spin of the local moment and that of the conduction electrons, $\mathbf{s}_{c,i}=(1/2)c_i^{\dagger}\boldsymbol{\sigma}c_i$, where $\boldsymbol{\sigma}$ denote the three Pauli matrices. Across the sites, the local moments are coupled to each other via an RKKY interaction I_{ij}.

The calculations that have provided the basis for the notion of Kondo destruction is the EDMFT[113–115]; for a recent review, see ref. 116. This approach treats the dynamical interplay between the Kondo and RKKY interactions of a Kondo-lattice described by panel **a**. The EDMFT approach corresponds to a non-perturbative summation of an infinite series of skeleton diagrams. They are generated by an effective action functional and are systematic and conserving.

In this approach, the fate of the Kondo-singlet amplitude is characterized by the nature of local correlation functions. The latter are determined from a Bose–Fermi Kondo/Anderson model:

$$\begin{aligned}H_{\mathrm{BFK}}=&\sum_{\mathbf{k},\sigma}E_{\mathbf{k}}c^{\dagger}_{\mathbf{k}\sigma}c_{\mathbf{k}\sigma}+\sum_{\mathbf{p}}\omega_{\mathbf{p}}\phi^{\dagger}_{\mathbf{p}}\phi_{\mathbf{p}}\\&+J_{\mathrm{K}}\mathbf{S}\cdot\frac{c_0^{\dagger}\boldsymbol{\sigma}c_0}{2}+g:\mathbf{S}:\cdot\sum_{\mathbf{p}}(\phi_{\mathbf{p}}+\phi^{\dagger}_{-\mathbf{p}})+h_{\mathrm{loc}}S^z.\end{aligned} \qquad (7)$$

Here the dispersion $E_{\mathbf{k}}$ and $\omega_{\mathbf{p}}$ are associated with a fermionic and a bosonic bath characterized by a fermionic field $c_{\mathbf{k}\sigma}$, at momentum **k** and spin σ, and a bosonic field $\phi_{\mathbf{p}}$, at momentum **p**. Their couplings to the local moment have the strength of J_{K} and *g*, respectively. In addition, h_{loc} denotes an effective static magnetic field, which is spontaneously generated and is coupled to the *z*-component of the local spin. Self-consistency equations are expressed in terms of the local correlators of the Bose–Fermi Kondo model.

The Kondo destruction is seen from the RG flow of the Bose–Fermi Kondo model. The RG is analysed at one loop from an ϵ expansion, first carried out in the model with Ising anisotropy[113] and subsequently extended to the model with SU(2) spin symmetry[117,118]. For the SU(2) and *xy*-spin symmetry cases, the RG analysis has been carried out to two and higher loops[119,120]. Here ϵ describes the power-law spectrum of the bosonic bath, which also contains a high-energy cutoff Λ:

$$\rho_{\mathrm{b}}(\omega)\equiv\sum_{\mathbf{p}}\delta(\omega-w_{\mathbf{p}})\propto|\omega|^{1-\epsilon}\quad\text{for }|\omega|<\Lambda. \qquad (8)$$

Panel **b** illustrates the flow that is associated with the RG beta-functions in the ϵ expansion, for a positive ϵ. The RG flow diagram illustrates two categories of stable fixed points: one associated with an infinite J_{K}, representing the Kondo screened phases, and the other characterized by $J_{\mathrm{K}}=0$, indicating Kondo-destroyed phases. An unstable fixed point corresponds to a Kondo-destruction QCP. In the absence of the bosonic Kondo coupling (when $g=0$), any non-zero J_{K} flows away from the decoupled fixed point and towards the Kondo fixed point[121]. The bosonic coupling *g* leads to two new fixed points and a separatrix in the J_{K}–g plane. The critical (red) fixed point controls the physics on the separatrix, corresponding to a critical destruction of the Kondo phase. On the right of the separatrix, the system flows to a Kondo-destroyed (green) fixed point where J_{K} vanishes altogether.

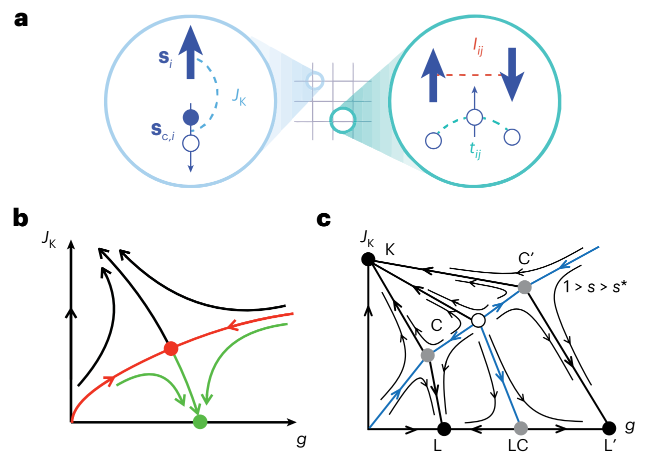

Kondo lattice model and renormalization-group fixed points. **a**, Schematic illustration of the Kondo-lattice model, which contains the Kondo coupling J_{K} between local moments and conduction electrons, hopping parameters t_{ij} between the conduction electrons, and RKKY interactions I_{ij} between the local moments. **b**,**c**, RG flow of the Bose–Fermi Kondo/Anderson model from studies based on an ϵ expansion[119] (**b**) and the continuous-time quantum Monte Carlo method[125] and a large-*S*-expansion approach[126] at 1>*s*> *s**, where *s** is the threshold value of the power-law exponent for the spectrum of the bosonic bath (see equation (8)). (**c**).In panel **c**, L and L′ mark two stable fixed points characterizing two local moment phases respectively, with LC denoting the quantum critical point between them. C and C′ characterize two Kondo-destruction quantum critical points between the local moment phases and the Kondo phase, which is denoted by K. Panels adapted with permission from: **a**, ref. 19, Springer Nature Ltd; **b**, ref. 119, APS; **c**, ref. 125, APS.

The nature of the critical (red) Kondo-destruction fixed point is to be contrasted with that of the Kondo fixed point. The Kondo fixed point is characterized by a non-zero Kondo-singlet amplitude, b^*, and the renormalized *f* electron energy scale, ε_f^*, for a pole[122,123] of the conduction-electron self-energy in energy space:

$$\Sigma(\mathbf{k},\omega)=\frac{(b^*)^2}{\omega-\varepsilon_f^*}. \qquad (9)$$

Here the self-energy is specified via the Dyson equation: $G_{\mathrm{c}}(\mathbf{k},\omega)=\left[\omega-\varepsilon_{\mathbf{k}}-\Sigma(\mathbf{k},\omega)\right]^{-1}$. Correspondingly, in the Kondo-lattice model, the conduction-electron Green's function contains two poles, respectively at energies

$$E^{\pm}_{\mathbf{k}}=\frac{1}{2}\left[\varepsilon_{\mathbf{k}}+\varepsilon_f^*\pm\sqrt{(\varepsilon_{\mathbf{k}}-\varepsilon_f^*)^2+4(b^*)^2}\right]. \qquad (10)$$

(continued from previous page)

They describe the heavy-fermion bands. The non-zero b^* specifies a Kondo resonance and leads to a large Fermi surface, where both the local moments and conduction electrons contribute. The quasiparticle weight is $Z_L \propto (b^*)^2$ (Fig. 5). The damping rate has the Fermi liquid $(k_BT)^2$ and E^2 form.

For the Kondo-destruction phenomena, we highlight three key characteristics. First, in the Kondo-destroyed phases, the Kondo-singlet amplitude b^* vanishes in the ground state. Consequently, the poles in the conduction-electron self-energy disappear, leading to a small Fermi surface for which only the conduction electrons contribute.

Second, for the Kondo-destruction QCP, the vanishing of the Kondo-singlet amplitude in the ground state implies that the weight of any Landau quasiparticle goes to zero. This can also be explicitly seen from the finite-size spectrum of the many-body excitations as determined by the numerical RG approach: the spectrum can no longer be fit in terms of a combination of any quasiparticles[124].

Third, the Kondo-destruction QCP is interacting (as opposed to being Gaussian). Thus, k_BT is the only energy scale. Accordingly, singular responses such as the local spin and charge susceptibilities have a dynamical Planckian ($\hbar\omega/k_BT$) scaling. This has been seen both in the Kondo-destruction fixed point of the Bose–Fermi Kondo/Anderson model as determined by a dynamical-large-N (where the index N appears in the spin channel) approach[66,68] and in the SU(2) case[66,124].

We note on the extra fixed points that exist beyond the ϵ expansion. It turns out that, for small ϵ, the SU(2) Bose–Fermi Kondo/Anderson model has more fixed points beyond those that are accessed by the ϵ-expansion method. Panel **c** shows the RG flow diagram when ϵ is sufficiently small (or $s = 1 - \epsilon$ is sufficiently large)[125]. As ϵ further increases, the fixed points are pair-wise annihilated, and this has recently been understood analytically based on a 1/S expansion (where S is the spin size)[126].

The stability of the $\mathrm{AF_S}$ phase has been analysed in terms of a quantum nonlinear sigma model representation of the Kondo lattice[36–39]. Using the $\mathrm{AF_S}$ phase as the starting point, there are three routes for quantum phase transitions to the paramagnetic heavy-fermion ($\mathrm{P_L}$) phase. Trajectory I describes a direct transition, with a Kondo-destruction QCP at the border of the AF order. Trajectory II passes through an intermediate $\mathrm{AF_L}$ phase, which corresponds to the SDW order from the heavy quasiparticles of the $\mathrm{P_L}$ phase. A Kondo-destruction transition takes place inside the AF order, while the QCP from the AF order to the paramagnetic phase is of the SDW type. Trajectory III passes through an intermediate $\mathrm{P_S}$ phase, which could involve non-magnetic order such as a valence-bond solid or an underlying spin liquid. Generically, the Luttinger theorem of the Kondo lattice is obeyed, as can be seen from how the local-moment part and conduction electrons[21,51] respond to the adiabatic insertion of an external flux[32]. The paramagnetic heavy-fermion phase itself, as described earlier, represents the standard phase of a Kondo lattice.

From the perspective of the paramagnetic heavy-fermion phase, the three trajectories of quantum phase transitions delineate a variety of ways for the Landau quasiparticles to be destroyed. Since the initial advancement of the global phase diagram[36], there has been considerable effort in exploring this phase diagram, both theoretically[37–43,52,53] and experimentally[46–50]. In addition to the Hall effect and quantum oscillations measurements, which we describe below, thermopower has been utilized to probe the Fermi surface reconstruction and elucidate the global phase diagram[54]. To illustrate the underlying physics, we will for the most part keep our discussion focused on the trajectory I of the global phase diagram, which is represented by the phase diagram shown in Fig. 3a in the space of temperature (T) and control parameter (δ).

Dynamical Planckian scaling

At the QCP, k_BT is the only energy scale, and this leads to dynamical properties in which $\hbar\omega$ scales with k_BT. The dynamical spin susceptibility at the AF wavevector $\mathbf{Q}$ is found[19,55] to have the following dynamical Planckian scaling form:

$$\chi(\mathbf{Q},\omega) = \frac{1}{(-\mathrm{i}\hbar\omega)^{\alpha}} W^{-1}\left(\frac{\hbar\omega}{k_BT}\right). \tag{1}$$

Here $W = A\,\mathcal{M}(\omega/T)$, with A being a constant prefactor and

$$\mathcal{M}(\omega/T) = \left(\frac{T}{-\mathrm{i}\omega}\right)^{\alpha} \exp[\,\alpha\,\psi(1/2 - \mathrm{i}\omega/2\pi T)\,], \tag{2}$$

where ψ is the digamma function.

The calculated exponent α is fractional, and is close to being 0.75 for the Ising anisotropic case (between 0.72 and 0.78 when different methods are used for the calculation)[56–59] and about 0.71 for the case with SU(2) spin symmetry[60]. At a general wavevector $\mathbf{q}$, the dynamical spin susceptibility takes the following form:

$$\chi(\mathbf{q},\omega) = \frac{1}{\theta(\mathbf{q}) + A\,(-\mathrm{i}\omega)^{\alpha}\mathcal{M}(\omega/T)}. \tag{3}$$

Here, $\theta(\mathbf{q}) = I_{\mathbf{Q}} - I_{\mathbf{q}}$, where $I_{\mathbf{q}}$ is the RKKY interaction expressed in wavevector space. The comparable critical exponents, obtained from calculations at the QCPs of the Ising anisotropic and SU(2)-symmetric Kondo-lattice models, imply the universal quantum critical behaviours of the dynamical spin susceptibility.

These theoretical results provide the understanding of the inelastic neutron-scattering data measured in $\mathrm{CeCu_{6-x}Au_x}$ at its quantum critical concentration $x_c = 0.1$ (ref. 25, see also ref. 26). The experiments show not only the $\hbar\omega/k_BT$ scaling form but also a fractional exponent $\alpha \approx 0.75$.

The Kondo-destruction QCP also predicted the temperature dependence of the NMR relaxation rate. When the hyperfine form factor does not have a strong dependence on the wavevector, the NMR relaxation rate $1/T_1$ is determined by the local spin susceptibility, leading to[19,55]:

$$\frac{1}{T_1} \propto \text{constant}. \tag{4}$$

In contrast, if the hyperfine coupling has a strong $\mathbf{q}$ dependence leading to a cancellation of the contributions from the dynamical spin susceptibility near the AF wavevector (as in the well-known case of the oxygen-site NMR relaxation rate of the optimally hole-doped cuprates[61,62]), the NMR relaxation rate has the following temperature dependence[63]:

$$\frac{1}{T_1} \propto T^{\alpha}. \tag{5}$$

The results from the silicon-site NMR experiments in $\mathrm{YbRh_2Si_2}$ found the NMR relaxation rate to be strongly dependent on the applied magnetic field[64,65]. When combined with the muon spin spectroscopy (μSR) results, they have allowed the extraction of the relaxation rate $1/T_1$ at the quantum critical magnetic field[63,64], and the result is consistent with the prediction of equation (4). Whereas the measured copper-site NMR relaxation rate in $\mathrm{CeCu_{6-x}Au_x}$, at the quantum critical concentration $x_c = 0.1$, is compatible with the expectation of equation (5)[63].

Importantly, charge response, particularly the optical conductivity, has also been found to be critical[27]. This would have been unusual for an SDW QCP, where the singular fluctuations are in the magnetic

https://doi.org/10.1038/s41567-024-02679-7

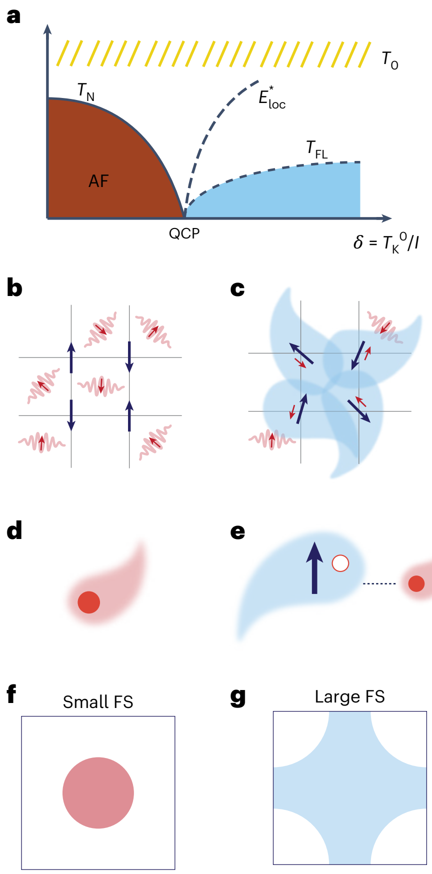

Fig. 3 | Kondo destruction quantum criticality and large-to-small Fermi surface transformation. **a**, Kondo-destruction quantum criticality of a Kondo lattice, in which a Kondo-destruction energy scale E^*_{loc} vanishes at the QCP. Here T_N, T_{FL} and T_0 denote the temperatures for an AF ordering, the crossover into a Fermi liquid state and the initial onset of Kondo correlations, respectively. **b**,**c**, On the two sides of the QCP are an AF order without the formation of a Kondo singlet (**b**) and a paramagnetic phase with a Kondo-singlet ground state (**c**). **d**,**e**, In the AF phase, the quasiparticles involve only the conduction electrons (**d**), in contrast to the paramagnetic phase, in which the Kondo singlets in the ground state yield composite heavy fermions in the excitation spectrum (**e**). **f**,**g**, The Fermi surface (FS) for the AF phase is small in that it involves only the conduction electrons (**f**), whereas that for the paramagnetic phase is large in that it also counts the number of local moments (**g**). Panels adapted with permission from: **a**, ref. 19, Springer Nature Ltd; **b**,**c**,**f**,**g**, ref. 2, Springer Nature Ltd.

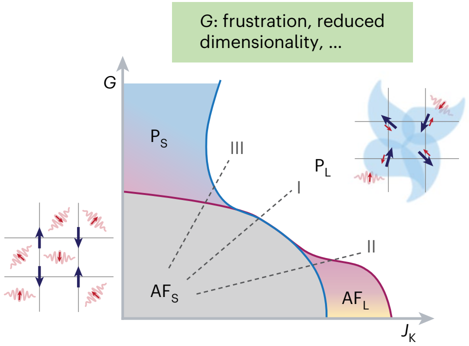

Fig. 4 | Global phase diagram for quantum critical phases and points from amplified quantum fluctuations. Global phase diagram of the heavy-fermion systems in the parameter space of J_K, the Kondo coupling, and G, which characterizes the quantum fluctuations in the local-moment magnetism. Figure adapted with permission from ref. 44, Wiley.

sector. Theoretically, at the Kondo-destruction QCP, the engagement of the Kondo process in the quantum criticality suggests the relevance of the single-particle and charge sectors to quantum criticality[66]. The corresponding responses, including the optical conductivity, obey dynamical Planckian scaling. Experimental evidence for the involvement of the charge sector in quantum criticality has also been provided in β-YbAlB$_4$ (ref. 67). Further evidence for a singular charge response has come from other theoretical studies[68–70].

Finally, as k_BT is the only energy scale at the QCP, the electronic scattering rate takes the form $1/\tau \propto (k_BT)/\hbar$. With the Umklapp scattering that is generically present in quantum critical metals, this relationship leads to strange-metal behaviour in the temperature dependence of the electrical resistivity.

Transformation of large-to-small Fermi surface and loss of quasiparticles

Large-to-small Fermi surface transformation across the QCP

An important characteristic of the Kondo-destruction quantum criticality is a transformation of a large to a small Fermi surface across the QCP. This turns out to be intimately connected to a loss of quasiparticles everywhere on the Fermi surface at the QCP. In the paramagnetic phase, the ground state has a non-zero amplitude of the Kondo singlet, describing the strength of the spin singlet between the local moments and conduction electrons, as illustrated in Fig. 3c. Correspondingly, composite-heavy-fermion excitations, as described by Fig. 3e, develop in the low-energy single-electron spectrum; as mentioned above, the Fermi surface is large in the sense that it incorporates both the conduction electrons and the Kondo-induced composite fermions, which we describe in Box 1.

On the other side of the QCP, the Kondo-singlet amplitude vanishes, as illustrated by Fig. 3b. The well-defined composite-fermion excitation is absent, and the single-particle excitations are entirely described by the renormalized conduction electrons as shown in Fig. 3d. This leads to a small Fermi surface as shown in Figs. 3f and 5a, which incorporates the conduction electrons only, as further described in Box 1.

The jump of the large-to-small Fermi surface across the QCP is experimentally testable[19–21,55,71]. Across the field-induced QCP in YbRh$_2$Si$_2$, a remarkable sequence of measurements[22,23] have identified a rapid isothermal crossover in the Hall coefficient (more specifically, the normal Hall coefficient). The crossover width extrapolates to zero in the $T = 0$ limit. This jump of the Hall coefficient provides evidence for a jump in the Fermi surface across the QCP. Moreover, the location of the crossover maps out a new temperature scale[22,23,72], as shown by the solid line in Fig. 1c. Separately, in CeRhIn$_5$, measurements of the de Haas–van Alphen effect have provided evidence of a sharp jump of the Fermi surface across the pressure-induced QCP[24]. Additional evidence for a Fermi-surface transformation across the QCP has come from Hall effect measurements in pressurized CeRhIn$_5$ (ref. 73).

Loss of quasiparticles at the QCP

As the system approaches the Kondo-destruction QCP from the side of a large Fermi surface, the Kondo-singlet amplitude goes to zero. The residue of the pole in the conduction-electron self-energy $\Sigma(\mathbf{k}, \omega)$ of equation (9) in Box 1 vanishes. Correspondingly, the quasiparticle weight on the large Fermi surface, Z_L vanishes, as illustrated in Fig. 5a. Continuity dictates that the quasiparticle weight on the small Fermi surface, Z_S, vanishes as well upon approaching the QCP from the other side of the phase diagram, as shown in Fig. 5a.

Direct spectral evidence of the destruction of quasiparticles at the QCP is hard to obtain because in heavy-fermion metals, angle-resolved photoemission spectroscopy measurements have yet to reach adequate resolution to address the issue. However, scanning tunnelling spectroscopy in the heavy-fermion compound YbRh$_2$Si$_2$ (ref. 74) has provided evidence that the single-particle excitations are

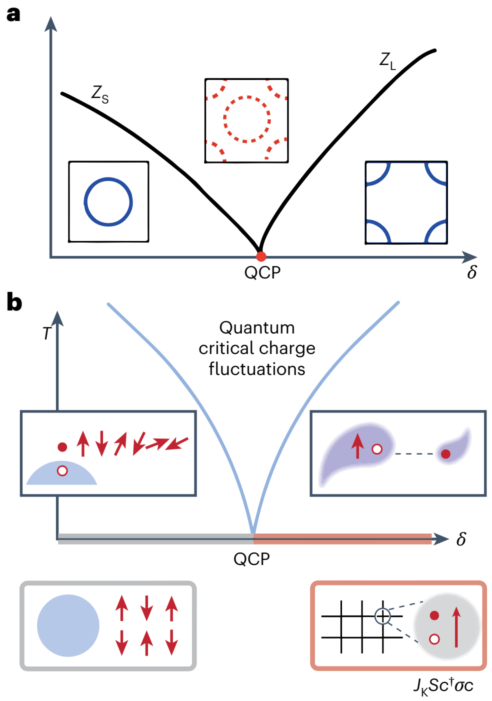

Fig. 5 | Loss of quasiparticles and quantum critical charge fluctuations. **a**, The quasiparticle spectral weight, Z_S and Z_L, for the small and large Fermi surfaces, respectively, as a function of δ, showing a large-to-small Fermi surface transformation across the Kondo-destruction QCP, and the loss of quasiparticles everywhere on the Fermi surface at the QCP[3]. **b**, Illustration of the quantum critical charge fluctuation at the Kondo-destruction QCP between an AF state, represented by the bottom left box where the staggered red arrows denote the long-range magnetic order of local moments and the blue circles represent the Fermi surface of the conduction electrons, and a paramagnetic state, indicated by the bottom-right box where a Kondo singlet is formed between the local moments (red arrow) and the spins of conduction electrons in the form of a spin-triplet combination of particles and holes (red solid and open dots). Panels adapted with permission from: **a**, ref. 3; APS **b**, ref. 27, AAAS.

a part of its quantum criticality[75]. Related evidence has come from the probe of Kondo-driven excitations in the quantum critical regime by time-resolved terahertz spectroscopy[76]. Recently, the current shot noise has been used as a new probe of strongly correlated metals. The observed reduction of the Fano factor provides fairly direct evidence for the loss of quasiparticles in the quantum critical regime of $YbRh_2Si_2$ (refs. 77,78).

Dynamical Kondo effect and high-T_c superconductivity as implications of the singular charge response

The fact that charge responses are singular and obey dynamical Planckian scaling at a magnetic QCP carries a special importance. It implicates a charge-spin entanglement in the Kondo-destruction quantum critical state, despite a vanishing amplitude of the Kondo singlet in the ground state. In fact, it has been shown that a dynamical Kondo correlation persists in this regime: a non-zero Kondo coupling in the Hamiltonian dictates that the cross local moment–conduction-electron spin correlations operate at non-zero frequencies[60]. More generally, recent work, both theoretical[79] and experimental[80], has provided evidence for amplified entanglement at the Kondo-destruction QCP.

Qualitatively, the Kondo-destruction QCP, described in Figs. 3 and 5, features quantum fluctuations between a phase that has a Kondo singlet in the ground state and with an accompanying large Fermi surface on the one hand, and a phase that has no Kondo singlet in the ground state and with a corresponding small Fermi surface on the other hand. As the composite heavy fermions carry both charge and spin, the fact that they are critically suppressed at the Kondo-destruction QCP means that the charge sector is an inherent component of the quantum criticality, as shown in Fig. 5b.

This dynamical Kondo effect has important implications for how unconventional superconductivity develops out of the strange-metal normal state. The Kondo-destruction quantum criticality is robust in that a large entropy—amounting to a substantial portion of $R\ln2$, where R is the ideal gas constant, per f site—is encoded in the quantum fluctuation spectrum. The primary degrees of freedom that are involved in this amplified quantum fluctuations are spin in nature. Indeed, a recent calculation using the cluster version of the extended dynamical mean-field theory (EDMFT) found large intersite spin-singlet correlations in this quantum critical fluid[81]. Through the dynamical Kondo effect, such amplified quantum fluctuations strongly influence the charge sector. In turn, the singlet spin correlations lead to pronounced spin-singlet pairing correlations. The calculations show that this process drives unconventional superconductivity with high-T_c: the transition temperature reaches a few per cent of the effective Fermi temperature[81].

Implications and broader contexts

Delocalization–localization transition in other correlated systems

We have emphasized how Kondo-destruction corresponds to a delocalization–localization transition of the f electrons across the QCP. Such an effect also appears in more complex f-electron systems, which involve entwined local degrees of freedom of both spins and orbitals[82–84]. Localization–delocalization transitions of this kind in a metallic environment is emerging as a unifying theme across the correlated material classes.

In the hole-doped cuprates, strange-metal behaviour is well established[85–90]. Hall effect measurements in $YBa_2Cu_3O_y$ (YBCO), when combined with the results in underdoped $La_{2-x}Sr_xCuO_4$ (LSCO) and overdoped $Tl_2Ba_2CuO_{6+\delta}$ have implicated a transition between phases with carrier concentrations p and $1+p$ near the optimal doping[91] (Fig. 6a). This is accompanied by the observation of mass enhancement in YBCO near optimal doping[92] (Fig. 6b). While this remains an issue of active discussions[93,94], the notion that the Fermi surface undergoes a small-to-large transformation as a function of hope doing has also been reported based on angle-dependent magnetoresistance measurements in $La_{1.6-x}Nd_{0.4}Sr_xCuO_4$ (ref. 95). Moreover, recent inelastic measurements have implicated a QCP near the optimal doping in LSCO[96]. All these provide evidence for the relevance of a QCP involving an electronic localization–delocalization to the physics of optimally hole-doped cuprates.

Evidence for a localization–delocalization transition has also been observed in other correlated electron material classes. For example, an orbital-selective Mott transition, with a large-to-small Fermi surface transformation, has been demonstrated in $FeTe_{1-x}Se_x$ by angle-resolved photoemission spectroscopy measurements[97], as shown in Fig. 6c,d. In a doped Mott insulator of organic charge-transfer salts, some preliminary evidence for a rapid Fermi surface change in a doped Mott insulator has also emerged from Hall[98] and thermoelectric[99] measurements. In moiré systems, related properties are also being uncovered[100,101]. Intriguingly, T_c/T_0 of the moiré systems is also on the order of a few per cent[100]. Finally, kagome and related metals with frustrated lattices, with active flat bands, have recently emerged as a platform for strange-metal behaviour[102–104]. A Kondo-lattice description[105,106] allows for strange metallicity in terms of localization–delocalization of electrons in compact molecular orbitals[107]; this approach leads to a phase diagram of temperature and control parameter that has now been supported by an experimentally determined temperature–pressure phase diagram in a kagome metal[108].

QCP versus quantum critical phase

One of the topical issues in the realm of quantum criticality concerns the possibility of a quantum critical phase. The global phase diagram

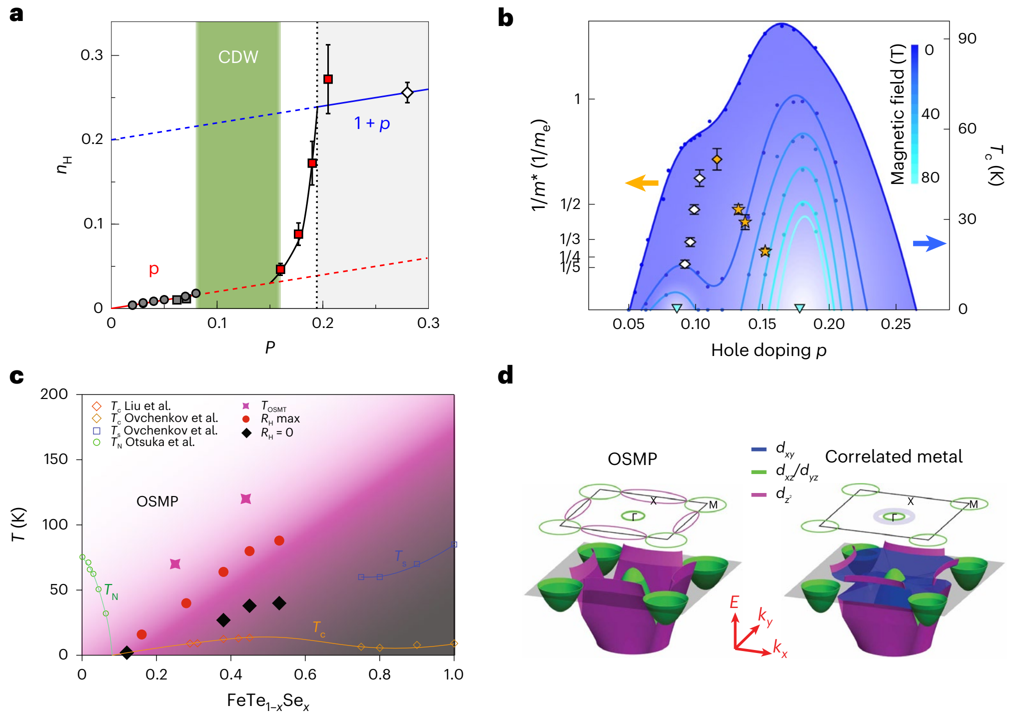

Fig. 6 | Evidence for localization–delocalization transitions in the cuprates and iron chalcogenides. a, Doping (p) dependence of the Hall number (n_H) in the hole-doped cuprates[91]. The red and blue lines correspond to $n_H = p$ and $n_H = 1 + p$ (with the error bars from measurements), respectively. The green region denotes the charge density wave (CDW) regime. **b**, Effective mass m^* (with its error bars from measurements), in the unit of bare electron mass (m_e), enhancement near the optimally doped YBCO under a high magnetic field, with the blue curves denoting T_c at different magnetic fields[92]. **c**, Phase diagram of $FeTe_{1-x}Se_x$, with T_N, T_s and T_c representing the temperatures for AF, structural and superconducting transitions, respectively. The red dots and black diamonds correspond to the temperatures for the maximum (R_H max) and zero ($R_H = 0$) Hall resistivity. The orbital-selective Mott transition temperature (T_{OSMT}) is defined as the temperature at which the photoemission spectral weight of the d_{xy} orbital vanishes. The gradual suppression of T_{OSMT} with decreasing x provides evidence for an orbital-selective Mott quantum phase transition. The panel incorporates data from refs. 127–129. **d**, Schematic illustration of a large-to-small Fermi surface transformation as x is decreased in $FeTe_{1-x}Se_x$, from a correlated metal phase to an orbital-selective Mott phase (OSMP), induced by the de-hybridization of the d_{xy} orbital associated with the OSMT[97]. Panels adapted with permission from: **a**, ref. 91, Springer Nature Ltd; **b**, ref. 92, AAAS; **c**,**d**, ref. 97 under a Creative Commons licence CC BY 4.0.

for quantum critical heavy-fermion metals, described earlier in the 'Global phase diagram' section and Fig. 4, delineates the close relationship between the two possibilities. Here a quantum critical phase can develop in the regime P_S, where quantum fluctuations prevent the system from acquiring a long-range order. The global phase diagram suggests that both the quantum critical phase and the beyond-Landau Kondo-destruction QCPs descend from the same phenomenon, namely, the strong dynamical competition between the Kondo and RKKY interactions. In a heavy-fermion compound with geometrical frustration (due to a distorted kagome lattice), CePdAl, a quantum critical phase has been implicated in its pressure–magnetic field phase diagram[47]. Evidence for a quantum critical phase has also come from thermoelectric measurements in an organic charge-transfer salt[99].

In the cuprates, we have already discussed evidence for the relevance of a QCP[91,92,95,96]. In the LSCO family, the evidence for a QCP developing near optimal superconductivity includes the observation of a peak in the specific heat (and, correspondingly, the maximization of entropy), and the presence of low-energy collective spin fluctuations with an energy scale comparable to temperature[96]. On the other hand, experimental observations have revealed that both the linear-T behaviour in the resistivity for LSCO[109,110] and a quadrature scaling in the magnetoresistance for $Tl_2Ba_2CuO_{6+\delta}$ and $Bi_2Sr_2CuO_{6+\delta}$ (ref. 110) occur at doping levels beyond p^*, raising the possibility of a quantum critical phase. Regardless of whether the physics is driven by a QCP or a quantum critical phase, the phenomenology suggests that both collective spin fluctuations and the electron localization–delocalization transition are involved in the low-energy physics in the strange-metal regime. This resembles the phenomena observed in heavy-fermion systems.

Summary and outlook

We have highlighted the theme that quasiparticles are fragile to begin with in strongly correlated metals such as heavy-fermion systems and that, in the Kondo-destruction quantum criticality, the quasiparticles are lost at the delocalization–localization transition of the f electrons. This theme unveils a hidden Mott transition in an unlikely setting, namely, between two metallic phases. As such, the unusualness of the properties here rivals what happens in the case of the standard Mott transition. By certain measure, it is even more striking because, with both sides of the transition being metallic, the Coulomb interactions are screened and it is more natural to have the quantum phase transition to be continuous. The loss of quasiparticles at the Kondo-destruction QCP is accompanied not only by the dynamical Planckian scaling in the spin and charge dynamics but also by a sudden transformation between large and small Fermi surfaces across the QCP.

These salient properties allow one to connect the strange metallicity of heavy-fermion metals with that of a variety of strongly correlated systems. The strange metallicity in the cuprates and organic systems naturally develop in the backdrop of the parent Mott insulator phase. In the iron-based superconductors, recent experiments have provided evidence for the proximate orbital-selective Mott phase. Finally, in moiré and frustrated lattice systems, where strange-metal behaviour has also been observed, correlated insulating phases may well be considered as the result of electron localization. It appears to be no coincidence that the strange-metal behaviour develops in all these strongly correlated material classes and that superconductivity emerges with a high transition temperature. By extension, it seems likely that, in most if not all of these systems, strange metallicity is underlined by the loss of quasiparticles on the entire Fermi surface. Exploring the issues in diverse settings and from varied perspectives promises to deepen the understanding about quantum critical metals and to uncover new connections that the strange-metal physics of heavy-fermion metals may have with that of a broad range of other correlated material classes.

References

1. Keimer, B. & Moore, J. E. The physics of quantum materials. *Nat. Phys.* **13**, 1045–1055 (2017).
2. Paschen, S. & Si, Q. Quantum phases driven by strong correlations. *Nat. Rev. Phys.* **3**, 9–26 (2021).
3. Kirchner, S. et al. Colloquium: Heavy-electron quantum criticality and single-particle spectroscopy. *Rev. Mod. Phys.* **92**, 011002 (2020).
4. Mathur, N. D. et al. Magnetically mediated superconductivity in heavy fermion compounds. *Nature* **394**, 39–43 (1998).
5. Zhu, L., Garst, M., Rosch, A. & Si, Q. Universally diverging Grueneisen parameter close to quantum critical points. *Phys. Rev. Lett.* **91**, 066404 (2003).
6. Wu, J., Zhu, L. & Si, Q. Entropy accumulation near quantum critical points: effects beyond hyperscaling. *J. Phys. Conf. Ser.* **273**, 012019 (2011).
7. Grube, K., Zaum, S., Stockert, O., Si, Q. & Löhneysen, H. V. Multidimensional entropy landscape of quantum criticality. *Nat. Phys.* **13**, 742–745 (2017).
8. Gegenwart, P. et al. Magnetic-field induced quantum critical point in $YbRh_2Si_2$. *Phys. Rev. Lett.* **89**, 056402 (2002).
9. Bruin, J. A. N., Sakai, H., Perry, R. S. & Mackenzie, A. P. Similarity of scattering rates in metals showing T-linear resistivity. *Science* **339**, 804–807 (2013).
10. Nguyen, D. H. et al. Superconductivity in an extreme strange metal. *Nat. Commun.* **12**, 4341 (2021).
11. Park, T. et al. Hidden magnetism and quantum criticality in the heavy fermion superconductor $CeRhIn_5$. *Nature* **440**, 65–68 (2006).
12. Knebel, G., Aoki, D., Brison, J.-P. & Flouquet, J. The quantum critical point in $CeRhIn_5$: a resistivity study. *J. Phys. Soc. Jpn* **77**, 114704 (2008).
13. Park, T. et al. Isotropic quantum scattering and unconventional superconductivity. *Nature* **456**, 366–368 (2008).
14. Hertz, J. Quantum critical phenomena. *Phys. Rev. B* **14**, 1165–1184 (1976).
15. Millis, A. J. Effect of a nonzero temperature on quantum critical points in itinerant fermion systems. *Phys. Rev. B* **48**, 7183–7196 (1993).
16. Hlubina, R. & Rice, T. M. Resistivity as a function of temperature for models with hot spots on the Fermi surface. *Phys. Rev. B* **51**, 9253–9260 (1995).
17. Rosch, A. Interplay of disorder and spin fluctuations in the resistivity near a quantum critical point. *Phys. Rev. Lett.* **82**, 4280–4283 (1999).
18. Borges, F., Borissov, A., Singh, A., Schlief, A. & Lee, S.-S. Field-theoretic functional renormalization group formalism for non-Fermi liquids and its application to the antiferromagnetic quantum critical metal in two dimensions. *Ann. Phys.* **450**, 169221 (2023).
19. Si, Q., Rabello, S., Ingersent, K. & Smith, J. Locally critical quantum phase transitions in strongly correlated metals. *Nature* **413**, 804–808 (2001).
20. Coleman, P., Pépin, C., Si, Q. & Ramazashvili, R. How do Fermi liquids get heavy and die? *J. Phys. Condens. Matter* **13**, R723 (2001).
21. Senthil, T., Vojta, M. & Sachdev, S. Weak magnetism and non-Fermi liquids near heavy-fermion critical points. *Phys. Rev. B* **69**, 035111 (2004).
22. Paschen, S. et al. Hall-effect evolution across a heavy-fermion quantum critical point. *Nature* **432**, 881–885 (2004).
23. Friedemann, S. et al. Fermi-surface collapse and dynamical scaling near a quantum-critical point. *Proc. Natl Acad. Sci. USA* **107**, 14547–14551 (2010).
24. Shishido, H., Settai, R., Harima, H. & Ōnuki, Y. A drastic change of the Fermi surface at a critical pressure in $CeRhIn_5$: dHvA study under pressure. *J. Phys. Soc. Jpn* **74**, 1103–1106 (2005).
25. Schröder, A. et al. Onset of antiferromagnetism in heavy-fermion metals. *Nature* **407**, 351–355 (2000).
26. Aronson, M. et al. Non-Fermi-liquid scaling of the magnetic response in $UCu_{5-x}Pd_x$ ($x = 1, 1.5$). *Phys. Rev. Lett.* **75**, 725–728 (1995).
27. Prochaska, L. et al. Singular charge fluctuations at a magnetic quantum critical point. *Science* **367**, 285–288 (2020).
28. Maksimovic, N. et al. Evidence for a delocalization quantum phase transition without symmetry breaking in $CeCoIn_5$. *Science* **375**, 76–81 (2022).
29. Nozieres, P. *Theory of Interacting Fermi Systems* (CRC Press, 2018).
30. Shankar, R. Renormalization-group approach to interacting fermions. *Rev. Mod. Phys.* **66**, 129–192 (1994).
31. Polchinski, J. Effective field theory and the Fermi surface. In *Proc. Theoretical Advanced Study Institute (TASI 92): From Black Holes and Strings to Particles* (eds Harvey, J. A. & Polchinski, J.) 235–276 (World Scientific, 1992).
32. Oshikawa, M. Topological approach to Luttinger's theorem and the Fermi surface of a Kondo lattice. *Phys. Rev. Lett.* **84**, 3370–3373 (2000).
33. Stewart, G. R. Non-Fermi-liquid behavior in *d*- and *f*-electron metals. *Rev. Mod. Phys.* **73**, 797–855 (2001).
34. Coleman, P. & Schofield, A. J. Quantum criticality. *Nature* **433**, 226–229 (2005).
35. Si, Q. & Steglich, F. Heavy fermions and quantum phase transitions. *Science* **329**, 1161–1166 (2010).
36. Si, Q. Global magnetic phase diagram and local quantum criticality in heavy fermion metals. *Physica B* **378**, 23–27 (2006).
37. Yamamoto, S. J. & Si, Q. Fermi surface and antiferromagnetism in the Kondo lattice: an asymptotically exact solution in $d > 1$ dimensions. *Phys. Rev. Lett.* **99**, 016401 (2007).
38. Ong, T. T. & Jones, B. A. Analysis of the antiferromagnetic phase transitions of the 2*d* Kondo lattice. *Phys. Rev. Lett.* **103**, 066405 (2009).
39. Yamamoto, S. J. & Si, Q. Global phase diagram of the Kondo lattice: from heavy fermion metals to Kondo insulators. *J. Low Tempe. Phys.* **161**, 233–262 (2010).
40. Goswami, P. & Si, Q. Effects of the Berry phase and instantons in one-dimensional Kondo–Heisenberg model. *Phys. Rev. Lett.* **107**, 126404 (2011).
41. Goswami, P. & Si, Q. Topological defects of Néel order and Kondo singlet formation for the Kondo–Heisenberg model on a honeycomb lattice. *Phys. Rev. B* **89**, 045124 (2014).
42. Goswami, P. & Si, Q. Dynamic zero modes of Dirac fermions and competing singlet phases of antiferromagnetic order. *Phys. Rev. B* **95**, 224438 (2017).
43. Liu, C.-C., Goswami, P. & Si, Q. Skyrmion defects and competing singlet orders in a half-filled antiferromagnetic Kondo–Heisenberg model on the honeycomb lattice. *Phys. Rev. B* **96**, 125101 (2017).
44. Si, Q. Quantum criticality and global phase diagram of magnetic heavy fermions. *Phys. Status Solidi B* **247**, 476–484 (2010).
45. Coleman, P. & Nevidomskyy, A. H. Frustration and the Kondo effect in heavy fermion materials. *J. Low Temp. Phys.* **161**, 182–202 (2010).

46. Custers, J. et al. Destruction of the Kondo effect in the cubic heavy-fermion compound $Ce_3Pd_{20}Si_6$. *Nat. Mater.* **11**, 189–194 (2012).
47. Zhao, H. et al. Quantum-critical phase from frustrated magnetism in a strongly correlated metal. *Nat. Phys.* **15**, 1261–1266 (2019).
48. Mun, E. D. et al. Magnetic-field-tuned quantum criticality of the heavy-fermion system YbPtBi. *Phys. Rev. B* **87**, 075120 (2013).
49. Kim, M. S. & Aronson, M. C. Spin liquids and antiferromagnetic order in the Shastry–Sutherland-lattice compound Yb_2Pt_2Pb. *Phys. Rev. Lett.* **110**, 017201 (2013).
50. Fritsch, V. et al. Approaching quantum criticality in a partially geometrically frustrated heavy-fermion metal. *Phys. Rev. B* **89**, 054416 (2014).
51. Pivovarov, E. & Si, Q. Transitions from small to large Fermi momenta in a one-dimensional Kondo lattice model. *Phys. Rev. B* **69**, 115104 (2004).
52. Pixley, J. H., Yu, R. & Si, Q. Quantum phases of the Shastry–Sutherland Kondo lattice: implications for the global phase diagram of heavy-fermion metals. *Phys. Rev. Lett.* **113**, 176402 (2014).
53. Sato, T., Assaad, F. F. & Grover, T. Quantum Monte Carlo simulation of frustrated Kondo lattice models. *Phys. Rev. Lett.* **120**, 107201 (2018).
54. Luo, Y. et al. Unconventional and conventional quantum criticalities in $CeRh_{0.58}Ir_{0.42}In5$. *npj Quantum Mater.* **3**, 6 (2018).
55. Si, Q., Rabello, S., Ingersent, K. & Smith, J. Local fluctuations in quantum critical metals. *Phys. Rev. B* **68**, 115103 (2003).
56. Grempel, D. & Si, Q. Locally critical point in an anisotropic Kondo lattice. *Phys. Rev. Lett.* **91**, 026401 (2003).
57. Zhu, J., Grempel, D. & Si, Q. Continuous quantum phase transition in a Kondo lattice model. *Phys. Rev. Lett.* **91**, 156404 (2003).
58. Glossop, M. & Ingersent, K. Magnetic quantum phase transition in an anisotropic Kondo lattice. *Phys. Rev. Lett.* **99**, 227203 (2007).
59. Zhu, J.-X., Kirchner, S., Bulla, R. & Si, Q. Zero-temperature magnetic transition in an easy-axis Kondo lattice model. *Phys. Rev. Lett.* **99**, 227204 (2007).
60. Hu, H., Cai, A. & Si, Q. Quantum criticality and dynamical Kondo effect in an SU(2) Anderson lattice model. Preprint at https://arxiv.org/abs/2004.04679 (2020).
61. Hammel, P. C., Takigawa, M., Heffner, R. H., Fisk, Z. & Ott, K. C. Spin dynamics at oxygen sites in $YBa_2Cu_3O_7$. *Phys. Rev. Lett.* **63**, 1992–1995 (1989).
62. Takigawa, M. et al. Cu and O NMR studies of the magnetic properties of $YBa_2Cu_3O_{6.63}$ (t_c=62 K). *Phys. Rev. B* **43**, 247–257 (1991).
63. Si, Q. The local quantum critical point and non-Fermi liquid properties. *J. Phys. Condens. Matter* **15**, S2207 (2003).
64. Ishida, K. et al. Low-temperature magnetic order and spin dynamics in $YbRh_2Si_2$. *Phys. Rev. B* **68**, 184401 (2003).
65. Ishida, K. et al. $YbRh_2Si_2$: spin fluctuations in the vicinity of a quantum critical point at low magnetic field. *Phys. Rev. Lett.* **89**, 107202 (2002).
66. Cai, A., Yu, Z., Hu, H., Kirchner, S. & Si, Q. Dynamical scaling of charge and spin responses at a Kondo destruction quantum critical point. *Phys. Rev. Lett.* **124**, 027205 (2020).
67. Kobayashi, H. et al. Observation of a critical charge mode in a strange metal. *Science* **379**, 908–912 (2023).
68. Zhu, L., Kirchner, S., Si, Q. & Georges, A. Quantum critical properties of the Bose–Fermi Kondo model in a large-*N* limit. *Phys. Rev. Lett.* **93**, 267201 (2004).
69. Pixley, J. H., Kirchner, S., Ingersent, K. & Si, Q. Kondo destruction and valence fluctuations in an Anderson model. *Phys. Rev. Lett.* **109**, 086403 (2012).
70. Komijani, Y. & Coleman, P. Emergent critical charge fluctuations at the Kondo breakdown of heavy fermions. *Phys. Rev. Lett.* **122**, 217001 (2019).
71. Pépin, C. Kondo breakdown as a selective mott transition in the Anderson lattice. *Phys. Rev. Lett.* **98**, 206401 (2007).
72. Gegenwart, P. et al. Multiple energy scales at a quantum critical point. *Science* **315**, 969–971 (2007).
73. Wang, H. et al. Evidence for charge delocalization crossover in the quantum critical superconductor $CeRhIn_5$. *Nat. Commun.* **14**, 7341 (2023).
74. Ernst, S. et al. Emerging local Kondo screening and spatial coherence in the heavy-fermion metal $YbRh_2Si_2$. *Nature* **474**, 362–366 (2011).
75. Seiro, S. et al. Evolution of the Kondo lattice and non-fermi liquid excitations in a heavy-fermion metal. *Nat. Commun.* **9**, 3324 (2018).
76. Yang, C.-J. et al. Critical slowing down near a magnetic quantum phase transition with fermionic breakdown. *Nat. Phys.* **19**, 1605–1610 (2023).
77. Chen, L. et al. Shot noise in a strange metal. *Science* **382**, 907–911 (2023).
78. Wang, Y. et al. Shot noise as a characterization of strongly correlated metals. Preprint at https://arxiv.org/abs/2211.11735 (2022).
79. Fang, Y. et al. Amplified entanglement witnessed in a quantum critical metal. Preprint at https://arxiv.org/abs/2402.18552 (2024).
80. Mazza, F. et al. Quantum Fisher information in a strange metal. Preprint at https://arxiv.org/abs/2403.12779 (2024).
81. Hu, H. et al. Unconventional superconductivity from Fermi surface fluctuations in strongly correlated metals. Preprint at https://arxiv.org/abs/2109.13224 (2021).
82. Martelli, V. et al. Sequential localization of a complex electron fluid. *Proc. Natl Acad. Sci. USA* **116**, 17701–17706 (2019).
83. Liu, C.-C., Paschen, S. & Si, Q. Quantum criticality enabled by intertwined degrees of freedom. *Proc. Natl Acad. Sci. USA* **120**, e2300903120 (2023).
84. Schultz, D. J., Han, SangEun & Kim, YongBaek Quantum impurity model for two-stage multipolar ordering and Fermi surface reconstruction. *Phys. Rev. B* **108**, L060401 (2023).
85. Legros, A. et al. Universal *T*-linear resistivity and Planckian dissipation in overdoped cuprates. *Nat. Phys.* **15**, 142–147 (2019).
86. Giraldo-Gallo, P. et al. Scale-invariant magnetoresistance in a cuprate superconductor. *Science* **361**, 479–481 (2018).
87. Takagi, H. et al. Systematic evolution of temperature-dependent resistivity in $La_{2-x}Sr_xCuO_4$. *Phys. Rev. Lett.* **69**, 2975 (1992).
88. Martin, S., Fiory, A. T., Fleming, R. M., Schneemeyer, L. F. & Waszczak, J. V. Normal-state transport properties of $Bi_{2+x}Sr_{2-y}CuO_{6+\delta}$ crystals. *Phys. Rev. B* **41**, 846–849 (1990).
89. Varma, C. M. Linear in temperature resistivity and associated mysteries including high temperature superconductivity. *Rev. Mod. Phys.* **92**, 031001 (2020).
90. Phillips, P. W., Hussey, N. E. & Abbamonte, P. Stranger than metals. *Science* **377**, eabh4273 (2022).
91. Badoux, S. et al. Change of carrier density at the pseudogap critical point of a cuprate superconductor. *Nature* **531**, 210–214 (2016).
92. Ramshaw, B. J. et al. Quasiparticle mass enhancement approaching optimal doping in a high-T_c superconductor. *Science* **348**, 317–320 (2015).
93. Putzke, C. et al. Reduced Hall carrier density in the overdoped strange metal regime of cuprate superconductors. *Nat. Phys.* **17**, 826–831 (2021).
94. Balakirev, F. F. et al. Signature of optimal doping in Hall-effect measurements on a high-temperature superconductor. *Nature* **424**, 912–915 (2003).
95. Fang, Y. et al. Fermi surface transformation at the pseudogap critical point of a cuprate superconductor. *Nat. Phys.* **18**, 558–564 (2022).

96. Zhu, M. et al. Spin fluctuations associated with the collapse of the pseudogap in a cuprate superconductor. *Nat. Phys.* **19**, 99–105 (2023).
97. Huang, J. et al. Correlation-driven electronic reconstruction in $FeTe_{1-x}Se_x$. *Commun. Phys.* **5**, 29 (2022).
98. Oike, H., Miyagawa, K., Taniguchi, H. & Kanoda, K. Pressure-induced Mott transition in an organic superconductor with a finite doping level. *Phys. Rev. Lett.* **114**, 067002 (2015).
99. Wakamatsu, K. et al. Thermoelectric signature of quantum critical phase in a doped spin-liquid candidate. *Nat. Commun.* **14**, 3679 (2023).
100. Cao, Y. et al. Unconventional superconductivity in magic-angle graphene superlattices. *Nature* **556**, 43–50 (2018).
101. Jaoui, A. et al. Quantum critical behaviour in magic-angle twisted bilayer graphene. *Nat. Phys.* **18**, 633–638 (2022).
102. Huang, J. et al. Non-Fermi liquid behaviour in a correlated flat-band pyrochlore lattice. *Nat. Phys.* **20**, 603–609 (2024).
103. Ye, L. et al. Hopping frustration-induced flat band and strange metallicity in a kagome metal. *Nat. Phys.* **20**, 610–614 (2024).
104. Ekahana, S. A. et al. Anomalous electrons in a metallic kagome ferromagnet. *Nature* **627**, 67–72 (2024).
105. Hu, H. & Si, Q. Coupled topological flat and wide bands: quasiparticle formation and destruction. *Sci. Adv.* **9**, eadg0028 (2023).
106. Chen, L. et al. Emergent flat band and topological kondo semimetal driven by orbital-selective correlations. *Nat. Commun.* **15**, 5242 (2024).
107. Chen, L. et al. Metallic quantum criticality enabled by flat bands in a kagome lattice. Preprint at https://arxiv.org/abs/2307.09431 (2023).
108. Liu, Y. et al. Superconductivity under pressure in a chromium-based kagome metal. *Nature* **632**, 1032–1037 (2024).
109. Cooper, R. A. et al. Anomalous criticality in the electrical resistivity of $La_{2-x}Sr_xCuO_4$. *Science* **323**, 603–607 (2009).
110. Ayres, J. et al. Incoherent transport across the strange-metal regime of overdoped cuprates. *Nature* **595**, 661–666 (2021).
111. Curro, N. J. et al. Unconventional superconductivity in $PuCoGa_5$. *Nature* **434**, 622–625 (2005).
112. Custers, J. et al. The break-up of heavy electrons at a quantum critical point. *Nature* **424**, 524–527 (2003).
113. Si, Q. & Smith, J. L. Kosterlitz–Thouless transition and short range spatial correlations in an extended Hubbard model. *Phys. Rev. Lett.* **77**, 3391–3394 (1996).
114. Smith, J. L. & Si, Q. Spatial correlations in dynamical mean-field theory. *Phys. Rev. B* **61**, 5184–5193 (2000).
115. Chitra, R. & Kotliar, G. Effective-action approach to strongly correlated fermion systems. *Phys. Rev. B* **63**, 115110 (2001).
116. Hu, H., Chen, L. & Si, Q. Extended dynamical mean field theory for correlated electron models. Preprint at https://arxiv.org/abs/2210.14197 (2022).
117. Smith, J. L. & Si, Q. Non-Fermi liquids in the two-band extended Hubbard model. *Europhys. Lett.* **45**, 228 (1999).
118. Sengupta, A. M. Spin in a fluctuating field: the Bose(+Fermi) Kondo models. *Phys. Rev. B* **61**, 4041–4043 (2000).
119. Zhu, L. & Si, Q. Critical local moment fluctuations in the Bose–Fermi Kondo model. *Phys. Rev. B* **66**, 024426 (2002).
120. Zaránd, G. & Demler, E. Quantum phase transitions in the Bose–Fermi Kondo model. *Phys. Rev. B* **66**, 024427 (2002).
121. Hewson, A. C. *The Kondo Problem to Heavy Fermions* (Cambridge Univ. Press, 1993).
122. Auerbach, A. & Levin, K. Kondo bosons and the Kondo lattice: microscopic basis for the heavy Fermi liquid. *Phys. Rev. Lett.* **35**, 3394–3414 (1987).
123. Millis, A. J. & Lee, P. A. Large-orbital-degeneracy expansion for the lattice Anderson model. *Phys. Rev. B* **35**, 3394–3414 (1987).
124. Kandala, A., Hu, H., Si, Q. & Ingersent, K. Dynamical Planckian scaling of charge response at a particle–hole-asymmetric quantum critical point with Kondo destruction. Preprint at https://arxiv.org/abs/2206.01174 (2022).
125. Cai, A. & Si, Q. Bose–Fermi Anderson model with SU(2) symmetry: continuous-time quantum Monte Carlo study. *Phys. Rev. B* **100**, 014439 (2019).
126. Hu, H. & Si, Q. Kondo destruction and fixed-point annihilation in a Bose–Fermi Kondo model. Preprint at https://arxiv.org/abs/2207.08744 (2022).
127. Liu, T. et al. From (π,0) magnetic order to superconductivity with (π,π) magnetic resonance in $Fe_{1.02}Te_{1-x}Se_x$. *Nat. Mater.* 9, 718–720 (2010).
128. Ovchenkov, Y. A. et al. Nematic properties of $FeSe_{1-x}Te_x$ crystals with a low Te content. Preprint at https://arxiv.org/abs/1909.00711 (2019).
129. Otsuka, T. et al. Incoherent-coherent crossover and the pseudogap in Te-annealed superconducting $Fe_{1+y}Te_{1-x}Se_x$ revealed by magnetotransport measurements. *Phys. Rev. B* **99**, 184505 (2019).

Acknowledgements

We thank A. Cai, J. Cano, L. Y. Chen, L. Deng, Y. Fang, M. T. Glossop, P. Goswami, the late D. R. Grempel, K. Grube, N. E. Hussey, K. Ingersent, A. Kandala, S. Kirchner, J. Kono, X.-W. Li, C.-C. Liu, M. B. Maple, D. Natelson, E. M. Nica, C. Pépin, J. H. Pixley, L. Prochaska, C. Setty, J. L. Smith, O. Stockert, S. Sur, J. D. Thompson, M. G. Vergniory, H. von Löhneysen, Y. Wang, S. Wirth, J.-D. Wu, R. Yu, F. Xie, J.-X. Zhu, L. J. Zhu and, particularly, S. Paschen and F. Steglich, for collaborations and discussions. We are grateful to J. D. Thompson for supplying Fig. 1a. This work has been supported in part by the NSF Grant number DMR-2220603 (H.H.), the AFOSR under Grant number FA9550-21-1-0356 (L.C.), the Robert A. Welch Foundation Grant No. C-1411 (Q.S.), the Vannevar Bush Faculty Fellowship ONR-VB N00014-23-1-2870 (Q.S.), and the European Research Council (ERC) under the European Union's Horizon 2020 research and innovation programme (Grant Agreement number 101020833) (H.H.).

Author contributions

H.H., L.C. and Q.S. contributed to the writing of the article.

Competing interests

The authors declare no competing interests.

Additional information

Correspondence and requests for materials should be addressed to Haoyu Hu, Lei Chen or Qimiao Si.

Peer review information *Nature Physics* thanks Manfred Fiebig and Tuson Park for their contribution to the peer review of this work.